

Determination of the basic timescale in kinetic Monte Carlo simulations by comparison with cyclic-voltammetry experiments

I. Abou Hamad^{a,b} P.A. Rikvold^{a,b,*} G. Brown^{b,c}

^a*Center for Materials Research and Technology and Department of Physics,
Florida State University, Tallahassee, FL 32306-4350, USA*

^b*School of Computational Science, Florida State University,
Tallahassee, FL 32306-4120, USA*

^c*Center for Computational Sciences, Oak Ridge National Laboratory,
Oak Ridge, TN 37831-6164, USA*

Abstract

While kinetic Monte Carlo simulations can provide long-time simulations of the dynamics of physical and chemical systems, it is not yet possible in general to identify the inverse Monte Carlo attempt frequency with a physical timescale in any but the simplest systems. Here we demonstrate such an identification by comparing simulations with experimental data. Using a dynamic lattice-gas model for the electroadsorption of Br on Ag(100), we measure the scan-rate dependence of the separation between positive- and negative-going peaks in cyclic voltammetry and compare simulated and experimental peak separations. By adjusting the Monte Carlo attempt frequency, good agreement between simulated and experimental peak separations is achieved. It is also found that the uniqueness of the determination depends on the relative values of the adsorption/desorption and diffusion free-energy barriers.

Key words: Monte Carlo Simulations, Non-equilibrium Thermodynamics and Statistical Mechanics, Adsorption Kinetics, Surface Diffusion, Bromine, Silver, Low Index Single Crystal Surfaces, Solid-Liquid Interfaces

PACS: 81.15.Pq, 82.20.Db, 82.20.Fd, 82.45.Qr, 05.10.Ln

* Corresponding author. Address: ^a Tel.: +1-850-644-6011; Fax: +1-850-644-0098
Email address: rikvold@csit.fsu.edu (P.A. Rikvold).

1 Introduction

At present, kinetic Monte Carlo (KMC) simulation is virtually the only computational method that enables numerical study of the dynamics of physical and chemical systems on macroscopically relevant timescales, anywhere from microseconds to millions of years [1,2,3,4,5]. However, the method is essentially a stochastic approximation to underlying classical or quantum mechanical processes on finer space and time scales [6,7]. It thus suffers from the problem that the basic MC timescale is often difficult to relate to an underlying physical timescale. While such a timescale could, in principle, be calculated from comparison with calculations at these finer scales [6], this is in practice rarely possible for electrochemical systems. Due to the complexity of the interactions with the solution, ab-initio methods can construct a reasonable horizontal corrugation potential [7] but give limited knowledge about the shape of the potential in the direction perpendicular to the surface. Moreover, water has effects both in terms of damping and in the shape of the adsorption/desorption free-energy barrier, which probably corresponds to a reconstruction of the solvation shell. While analytic macroscopic theories can be derived in terms of MC parameters [8], such theories cannot directly predict the values of those parameters. A rough estimate of the overall reaction rate constant can be obtained by applying standard electrochemical techniques [9] to the experimental data. Yet, the overall reaction rate gives little information, if any, about the free-energy barrier heights for the different processes of adsorption/desorption and surface diffusion.

Here we present an alternative approach: comparison of KMC results with time-dependent experimental results. In particular, we compare KMC simulations of a lattice-gas model with experimental results for cyclic-voltammetry (CV) studies of the electrosorption of Br on single-crystal Ag(100) surfaces. The lattice-gas model represents the long-lived configurations of adsorbed Br, and an MC step corresponds to an attempt at hopping across a saddle point in the free-energy landscape to a new configuration [7].

The Br/Ag(100) system has a phase transition (in the two-dimensional Ising universality class) between a disordered phase at more negative potentials and an ordered $c(2 \times 2)$ phase at more positive potentials [10]. The phase transition is associated with a divergence of the coverage fluctuations, corresponding to a peak in the cyclic voltammogram. The same phase transition has also been observed for Cl/Ag(100) in electrochemical [11] and ultra-high vacuum (UHV) environments [12,13].

Recent static and kinetic MC studies have been used to investigate the phase ordering and disordering mechanisms in cyclic-voltammetry (CV) and sudden potential-step experiments for halide adsorption on Ag(100) [14,15]. As the

CV scan rate is increased, the system is driven further from equilibrium. As a result, there is a widening of the separation between the positions of the CV peak for the positive-going and the negative-going scan of the electrode potential (in experiments) or the electrochemical potential (in simulations). Experimental peak separations have been measured for different sweep rates of the electrode potential [16]. When these experimental values, with time measured in seconds, are compared to the simulations, with time measured in Monte Carlo steps per site (MCSS), a physical time can be associated with the inverse MC attempt frequency. This was previously attempted by Mitchell *et al.* [17], but simulations at that time could not achieve peak separations within the experimental range. Due to the increase in computer power and to a new mean-field enhanced simulation method that we developed for calculating long-range interactions [11], it is now possible to simulate peak separations well within the experimental range.

2 Lattice-gas Model

We employ a LG model similar to that used by Koper [18,19] and Mitchell, *et al.* [14,15]. The Br ions adsorb on four-fold hollow sites of the Ag(100) surface [7,20]. The model is defined by the grand-canonical effective Hamiltonian,

$$\mathcal{H} = - \sum_{i<j} \phi_{ij} c_i c_j - \bar{\mu} \sum_{i=1}^N c_i, \quad (1)$$

where $\sum_{i<j}$ is a sum over all pairs of sites, ϕ_{ij} are the lateral interactions between particles on the i th and j th lattice sites measured in meV/pair, $\bar{\mu}$ is the electrochemical potential measured in meV/particle, and $N = L^2$ is the total number of lattice sites. The local occupation variables c_i can take the values 1 or 0, depending on whether site i is occupied by an ion (1) or empty (0).

The simulations were performed on $L \times L$ square lattices, using periodic boundary conditions to reduce finite-size effects. The interaction constants ϕ_{ij} between ions on sites i and j a distance r_{ij} apart (measured in units of the Ag(100) lattice spacing, $a = 2.889 \text{ \AA}$ [10]) are given by

$$\phi_{ij} = -\infty \times \delta_{r_{ij},1} + \frac{2^{3/2} \phi_{\text{nnn}}}{r_{ij}^3}, \quad (2)$$

where $\delta_{r_{ij},1}$ is a Kronecker delta with the infinitely negative value for $r_{ij} = 1$ indicating nearest-neighbor exclusion. Negative values of ϕ_{nnn} denote long-range repulsion. The interactions for large r_{ij} are most likely of electrostatic

dipole-dipole nature [21], but may also have a component mediated by the Ag substrate [22] that may not be uniformly repulsive.

Assuming a sufficient concentration of counterions in the electrolyte, the electrochemical potential $\bar{\mu}$ is, in the dilute-solution approximation, related to the bulk ionic concentration C and the electrode potential E (measured in mV) as

$$\bar{\mu} = \bar{\mu}_0 + k_{\text{B}}T \ln \frac{C}{C_0} - e\gamma E, \quad (3)$$

where $\bar{\mu}_0$ is an arbitrary constant, C_0 is a reference concentration (here 1 mM), $k_{\text{B}}T$ is Boltzmann's constant times the temperature, and e is the elementary charge unit. The electrosorption valency γ [23,24] (here assumed constant [11,21]) corresponds to the fraction of the ionic charge transferred during the adsorption process. We use the sign convention that $\bar{\mu} > 0$ favors adsorption.

The adsorbate coverage is defined as $\theta = N^{-1} \sum_{i=1}^N c_i$. It can be experimentally obtained by standard electrochemical methods, as well as from the integer-order peaks in surface X-ray scattering (SXS) data [10,25]. The derivative of the coverage with respect to the electrochemical potential, $d\theta/d\bar{\mu}$, is proportional to the current density in an experimental CV as described in section 4.

We have previously estimated the next-nearest-neighbor lateral interaction energy ($\phi_{\text{nnn}} \approx -21$ meV) and the electrosorption valency ($\gamma \approx -0.72$), based on fits of simulated equilibrium adsorption isotherms to experimental data [11]. Remarkably, despite the very different environments this value of ϕ_{nnn} , estimated from the shape of the adsorption isotherms, is consistent to within 10% with the one obtained from the temperature dependence of the critical coverage for Cl/Ag(100) in UHV [12,13]. In the next section we detail the kinetic MC approach.

3 Kinetic Monte Carlo Method

Kinetic Monte Carlo simulations were performed on systems with $L = 128$, and the absence of significant finite-size effects was verified by additional simulations for $L = 64$ and 256. The kinetic MC simulation proceeds as follows. We randomly select a lattice site i , and depending on the occupation c_i , different moves are attempted. If $c_i = 0$, only adsorption is attempted, while if $c_i = 1$, 9 different moves are proposed: desorption, diffusion to each of the 4 nearest-neighbor sites, and diffusion to each of the 4 next-nearest-neighbor

sites. Next, a weighted list for accepting each of these moves is constructed using Eq. (5) below, to calculate the probabilities $R(\text{F}|\text{I})$ of the individual moves between the initial state I and final state F. The probability for the system to stay in the initial configuration is consequently $R(\text{I}|\text{I}) = 1 - \sum_{\text{F} \neq \text{I}} R(\text{F}|\text{I})$ [15].

Using a thermally activated, stochastic barrier-hopping picture, the energy of the transition state for a microscopic change from an initial state I to a final state F is approximated by the symmetric Butler-Volmer formula [2,26,27]

$$U_{\text{T}_\lambda} = \frac{U_{\text{I}} + U_{\text{F}}}{2} + \Delta_\lambda, \quad (4)$$

where U_{I} and U_{F} are the energies of the initial and final states, respectively, T_λ is the transition state for process λ , and Δ_λ is a “bare” barrier associated with process λ , which here can be one of nearest-neighbor diffusion (Δ_{nn}), next-nearest-neighbor diffusion (Δ_{nnn}), or adsorption/desorption ($\Delta_{\text{a/d}}$).

The probability for a particle to make a transition from state I to state F is approximated by the one-step Arrhenius rate [2,26,27]

$$\mathcal{R}(\text{F}|\text{I}) = \nu \exp\left(-\frac{\Delta_\lambda}{k_{\text{B}}\text{T}}\right) \exp\left(-\frac{U_{\text{F}} - U_{\text{I}}}{2k_{\text{B}}\text{T}}\right), \quad (5)$$

where ν is the attempt frequency, which sets the overall timescale for the simulation. This formalism assumes that all processes λ have the same MC attempt frequency of 1 MCSS⁻¹. Although this assumption may not be true in general [28], because different processes involve different potential wells and thus different vibrational frequencies, it can be used to find an effective timescale conversion between MC time and physical time, given the MC attempt frequencies. The MC time unit, one MCSS, corresponds to the attempted update of N randomly chosen sites. For a simulation with scan rate ρ (in meV/MCSS), $\bar{\mu}$ is incremented by $(\rho \times 1 \text{ MCSS})$ meV every MCSS until it reaches its final value, and then decremented back to its initial value.

Since the value of $U_{\text{F}} - U_{\text{I}}$ determines \mathcal{R} in Eq. (5), the approximations made to calculate the large- r contributions to the pair sum in Eq. (1) are important. In our simulations, to calculate the energy changes we included the exact contributions for particle separations up to $r_{ij} = 3$, while using a mean-field approximation for larger separations [11].¹

¹ Omission of the mean-field part, which could be viewed as a simple-minded way to introduce electrostatic screening, would increase the value of ϕ_{nnn} that best fits the equilibrium isotherms by 5 – 10% [11,21].

4 Results

Starting at an initial potential of $\bar{\mu} = -200$ meV and room temperature ($\beta = 1/k_{\text{B}}T = 0.04$ meV $^{-1}$), the MC process discussed in Sec. 3 was repeated until $\bar{\mu}$ reached +600 meV, and then decremented at the same rate back to -200 meV. The coverage isotherms were computed using scan rates ranging over four decades, from $\rho = 3 \times 10^{-5}$ to 0.1 meV/MCSS, and for $\Delta_{\text{a/d}} = 150, 175, 200, 250, 300, 350,$ and 400 meV. The other barriers, $\Delta_{\text{nmn}} = 200$ meV and $\Delta_{\text{nn}} = 100$ meV, were kept constant at the values determined by comparison with density-functional theory calculations [7,20]. The hysteresis loops for θ as a function of E are shown for $\Delta_{\text{a/d}} = 300$ meV in Fig. 1 for different scan rates. Each loop was averaged over eight independent simulation runs.

Next, the Savitzky-Golay method [29,30] with a second-order polynomial and a window of 51 points was used to obtain the smoothed numerical derivative $d\theta/d\bar{\mu}$, which is proportional to the simulated CV current density j [15]:

$$j = \frac{\gamma^2 e^2}{A_s} \frac{d\theta}{d\bar{\mu}} \frac{dE}{dt}, \quad (6)$$

where A_s is the area of one adsorption site. Consequently, the differential adsorption capacitance per unit area becomes

$$C = \frac{j}{dE/dt} = \frac{\gamma^2 e^2}{A_s} \frac{d\theta}{d\bar{\mu}}. \quad (7)$$

As seen in Fig. 2, the difference between the positions of the positive-going and negative-going peaks depends on the scan rate. This difference is due to two physical effects. First, jamming due to the nearest-neighbor exclusion, which is only slowly alleviated by lateral diffusion [15], causes the coverage to lag behind its equilibrium value. Second, critical slowing down also causes the coverage to equilibrate slowly near the phase transition at the CV peak [15].²

By fitting the separation of the positive-going scan peak (E_p) and the negative-going scan peak (E_n) of the simulated CVs to experimental data for $E_p - E_n$ vs dE/dt [16], we can extract a physical time τ corresponding to 1 MCSS (the inverse MC attempt frequency, $\tau = 1/\nu$) for each value of the adsorption/desorption free-energy barrier height $\Delta_{\text{a/d}}$. A χ^2 which measures the square of the horizontal differences between the experimental curves and the

² If j is plotted vs θ , rather than vs E or $\bar{\mu}$, all the peaks fall in the range $0.37 \leq \theta \leq 0.40$ for positive-going scans and $0.33 \leq \theta \leq 0.37$ for negative-going scans. This is consistent with the values of the hard-square jamming coverage and critical coverage [12,13,15].

simulated peak separations, multiplied by trial values of τ , was calculated. The value of τ which minimized χ^2 was taken to be the best-fit value. See Fig. 3. For $\Delta_{a/d} \leq 350$ meV, the simulations were fit to the experimental data points, while for $\Delta_{a/d} = 400$ meV the simulations were fit to the best-fit simulated data points for $\Delta_{a/d} = 300$ meV since the peak separations attainable for $\Delta_{a/d} = 400$ meV are not within the experimental data range. The fits for most values of $\Delta_{a/d}$ coincide to within the accuracy of the experimental data and our statistics. Yet, focusing on the experimental data range (inset in Fig. 3), suggests that $\Delta_{a/d} = 175$ meV and $\tau = 5.3 \times 10^{-6}$ s fits best to the experimental data. This distinction relies mainly on the two experimental data points corresponding to the highest scan rates and thus would be better founded if there were more experimental data in that range. In addition, since the simulated curves for $\Delta_{a/d} > 200$ meV practically coincide, it is only for $\Delta_{a/d} \leq 200$ meV that a clear distinction can be made among the different $\Delta_{a/d}$ values, even with more accurate experimental data.

For $\Delta_{a/d} > 200$ meV, the physical time τ corresponding to one MCSS is simply related to $\Delta_{a/d}$ as seen in Fig. 4. The relationship between τ and $\Delta_{a/d}$ is related to the Arrhenius form:

$$\tau = \tau_0 \exp(-\beta \Delta_{a/d}) , \quad (8)$$

or

$$\log_{10}(\tau/s) = (\ln(\tau_0/s) - \beta \Delta_{a/d}) / \ln 10. \quad (9)$$

Plotting $\log_{10}(\tau/s)$ vs $\Delta_{a/d}$ results in a straight line with a slope of -0.0388 meV $^{-1}/\ln 10$ (excluding $\Delta_{a/d} = 150$ and 175 meV), in very good agreement with what is expected from Eq. (9) with the inverse temperature used, $\beta = 0.04$ meV $^{-1}$. We also find that, as $\Delta_{a/d}$ decreases and becomes comparable to Δ_{mn} and Δ_{nn} , diffusion becomes relatively more important in determining the overall timescale, and the dependence of τ on $\Delta_{a/d}$ deviates from Eq. (9). This deviation makes differentiation among different values of $\Delta_{a/d}$ easier because in this limit a change in $\Delta_{a/d}$ cannot be compensated by a change in τ , and the details of the dynamics directly influence the peak separation.

5 Conclusions

By comparing with experiments simulations at potential-scan rates sufficiently slow to produce peak separations that fall within the experimental range, we

were able to extract a physical timescale associated with the inverse MC attempt frequency $\tau = 5.3 \times 10^{-6}$ s, a value much larger than normally expected. This may be the result of relatively flat potential minima for the adsorption process, possibly related to reorganization of the ion hydration shells. Another possible reason is the assumption that all processes in the MC have the same attempt frequency; different processes could, in general, have different MC attempt frequencies. Thus τ would correspond to an effective inverse MC attempt frequency for an overall process.

For values of the adsorption/desorption free-energy barrier $\Delta_{a/d}$ that are large compared to the diffusion barriers ($\Delta_{a/d} \geq 200$ meV), the relationship between τ and $\Delta_{a/d}$ is consistent with the Arrhenius law. Under such conditions the process of Br adsorption/desorption controls the dynamics in this electrochemical system, and the possible difference in attempt frequencies for different processes becomes less important. For situations in which $\Delta_{a/d}$ is comparable to the values of the lateral diffusion of adsorbates on the substrate, deviations from the Arrhenius law appear. Then no process is dominant. In conclusion we have here shown that simulations which measure the competition between these processes can be used to distinguish between different $\Delta_{a/d}$ values by comparison to experiments.

Acknowledgments

We thank J.X. Wang for supplying us with the experimental data, S.J. Mitchell for useful discussions, and A.P.J. Jansen for helpful comments. This work was supported in part by NSF grant No. DMR-0240078 and by Florida State University through the School of Computational Science and the Center for Materials Research and Technology.

References

- [1] M. Kolesik, M.A. Novotny, P.A. Rikvold, *Int. J. Mod. Phys. C* 14 (2003) 121.
- [2] G. Brown, P.A. Rikvold, S.J. Mitchell, M.A. Novotny, in: A. Wieckowski (Ed.), *Interfacial Electrochemistry: Theory, Experiment, and Applications*, Marcel Dekker, New York, 1999, p. 47.
- [3] N. Combe, P. Jensen, A. Pimpinelli, *Phys. Rev. Lett.* 85 (2000) 110.
- [4] S. Auer, D. Frenkel, *Nature (London)* 409 (2001) 1020.
- [5] M.A. Novotny, G. Brown, P.A. Rikvold, *J. Appl. Phys.* 91 (2002) 6908.

- [6] U. Nowak, R.W. Chantrell, E.C. Kennedy, *Phys. Rev. Lett.* 84 (2000) 163.
- [7] S.J. Mitchell, S. Wang, P.A. Rikvold, *Faraday Disc.* 121 (2002) 53.
- [8] F. Berthier, B. Legrand, J. Creuze, R. Tétot, *J. Electroanal. Chem.* 561 (2004) 37; *J. Electroanal. Chem.* 562 (2004) 127, and references therein.
- [9] S. Srinivasan, E. Gileadi, *Electrochim. Acta* 11 (1966) 321.
- [10] B.M. Ocko, J.X. Wang, Th. Wandlowski, *Phys. Rev. Lett.* 79 (1997) 1511.
- [11] I. Abou Hamad, Th. Wandlowski, G. Brown, P.A. Rikvold, *J. Electroanal. Chem.* 554 (2003) 211.
- [12] D.E. Taylor, E.D. Williams, R.L. Park, N.C. Bartelt, T.E. Einstein, *Phys. Rev. B* 32 (1985) 4653.
- [13] R.Q. Hwang, E.D. Williams, N.C. Bartelt, R.L. Park, *Phys. Rev. B* 37 (1988) 5870.
- [14] S.J. Mitchell, G. Brown, P.A. Rikvold, *J. Electroanal. Chem.* 493 (2000) 68.
- [15] S.J. Mitchell, G. Brown, P.A. Rikvold, *Surf. Sci.* 471 (2001) 125.
- [16] J.X. Wang, private communication.
- [17] S.J. Mitchell, P.A. Rikvold, G. Brown, in: *Computer Simulation Studies in Condensed Matter Physics XIII*, edited by D.P. Landau, S.P. Lewis, and H.-B. Schüttler, *Springer Proceedings in Physics Vol. 86* (Springer, Berlin, 2001) p. 189.
- [18] M.T.M. Koper, *J. Electroanal. Chem.* 450 (1998) 189.
- [19] M.T.M. Koper, *Electrochim. Acta* 44 (1998) 1207.
- [20] S. Wang, P.A. Rikvold, *Phys. Rev. B* 65 (2002) 155406.
- [21] I. Abou Hamad, S.J. Mitchell, Th. Wandlowski, P.A. Rikvold, G. Brown in preparation.
- [22] T.L. Einstein, *Langmuir*, 7 (1991) 2520.
- [23] K.J. Vetter, J.W. Schultze, *Ber. Bunsenges. Phys. Chem.* 76 (1972) 920; *Ber. Bunsenges. Phys. Chem.* 76 (1972) 927.
- [24] W. Schmickler, *Interfacial Electrochemistry*, Oxford University Press, New York, 1996.
- [25] Th. Wandlowski, J.X. Wang, B.M. Ocko, *J. Electroanal. Chem.* 500 (2001) 418.
- [26] H.C. Kang, W.H. Weinberg, *J. Chem. Phys.* 90 (1989) 2824.
- [27] G.M. Buendía, P.A. Rikvold, K. Park, M.A. Novotny, *J. Chem. Phys.* 121 (2004) 4193, and references therein.
- [28] A.M. Bowler, E.S. Hood, *J. Chem. Phys.* 94 (1991) 5162.

- [29] A. Savitzky, M.J.E. Golay, *Anal. Chem.* 36 (1964) 1627.
- [30] W.H. Press, A. Teukolsky, W.T. Vetterling, B.P. Flannery: *Numerical recipes in C: the art of scientific computing*, Cambridge University Press (1997).

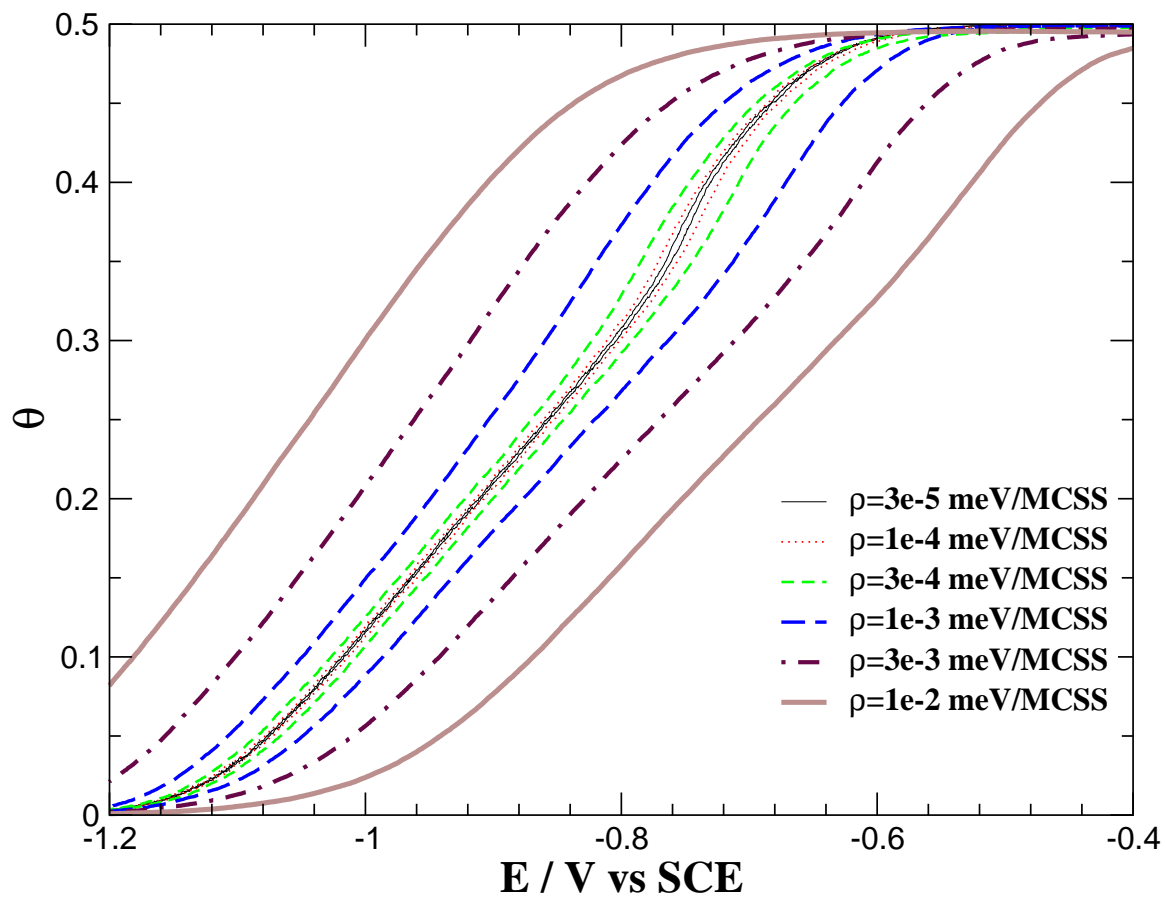


Fig. 1. The coverage θ as a function of the electrode potential E for $\Delta_{a/d} = 300 \text{ meV}$ and different scan rates.

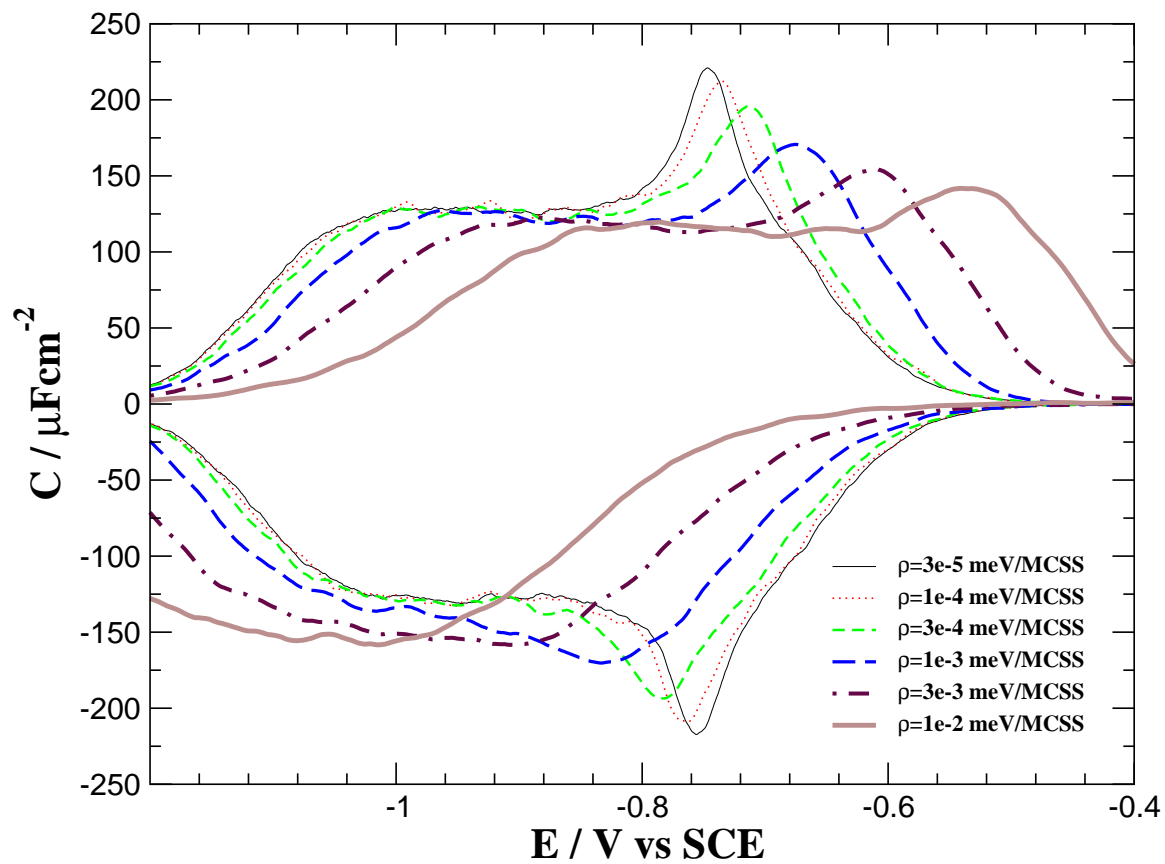


Fig. 2. Simulated adsorption capacitance cyclic voltammograms for $\Delta_{a/d} = 300 \text{ meV}$ and different scan rates.

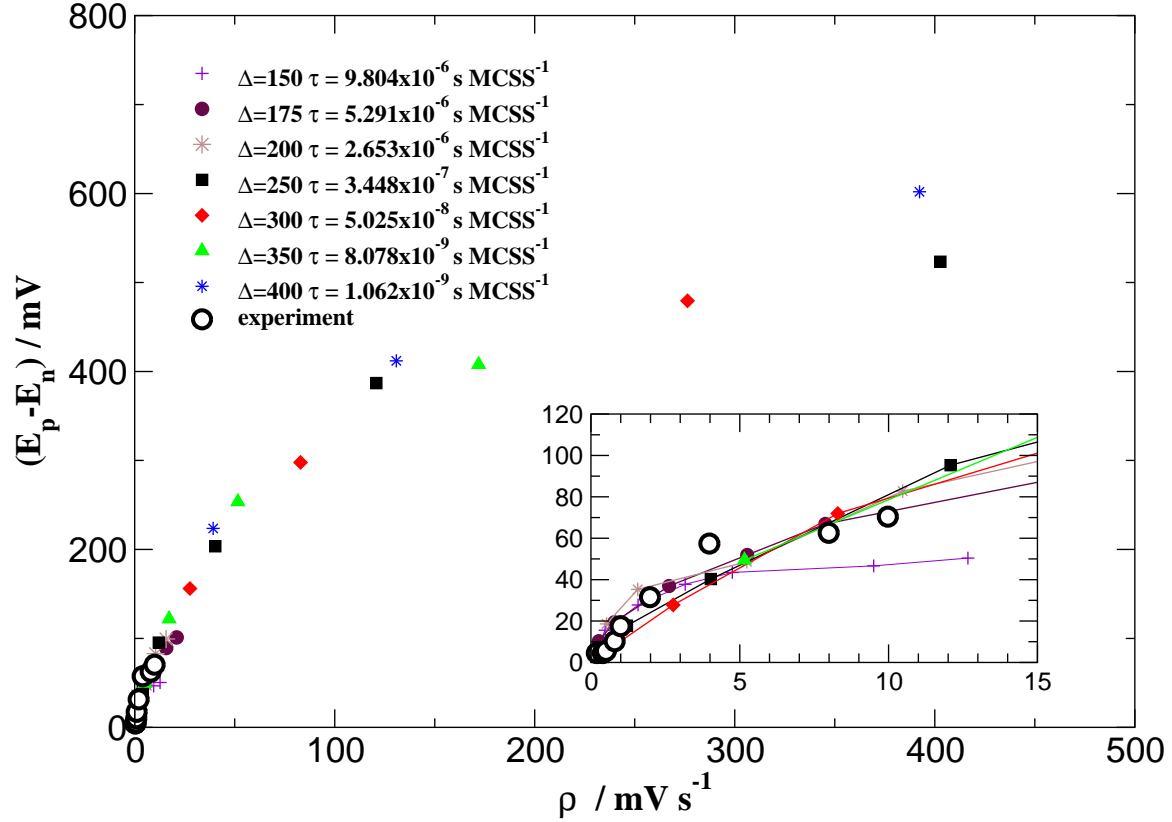


Fig. 3. Fits of kinetic MC simulations to experimental peak separations using different values for the adsorption-desorption barrier, $\Delta_{a/d}$. Zooming into the experimental data range (inset) suggests that the best-fit value for $\Delta_{a/d}$ is 175 meV, corresponding to $\tau \approx 5.3 \times 10^{-6}$ s. The lines are guides to the eye.

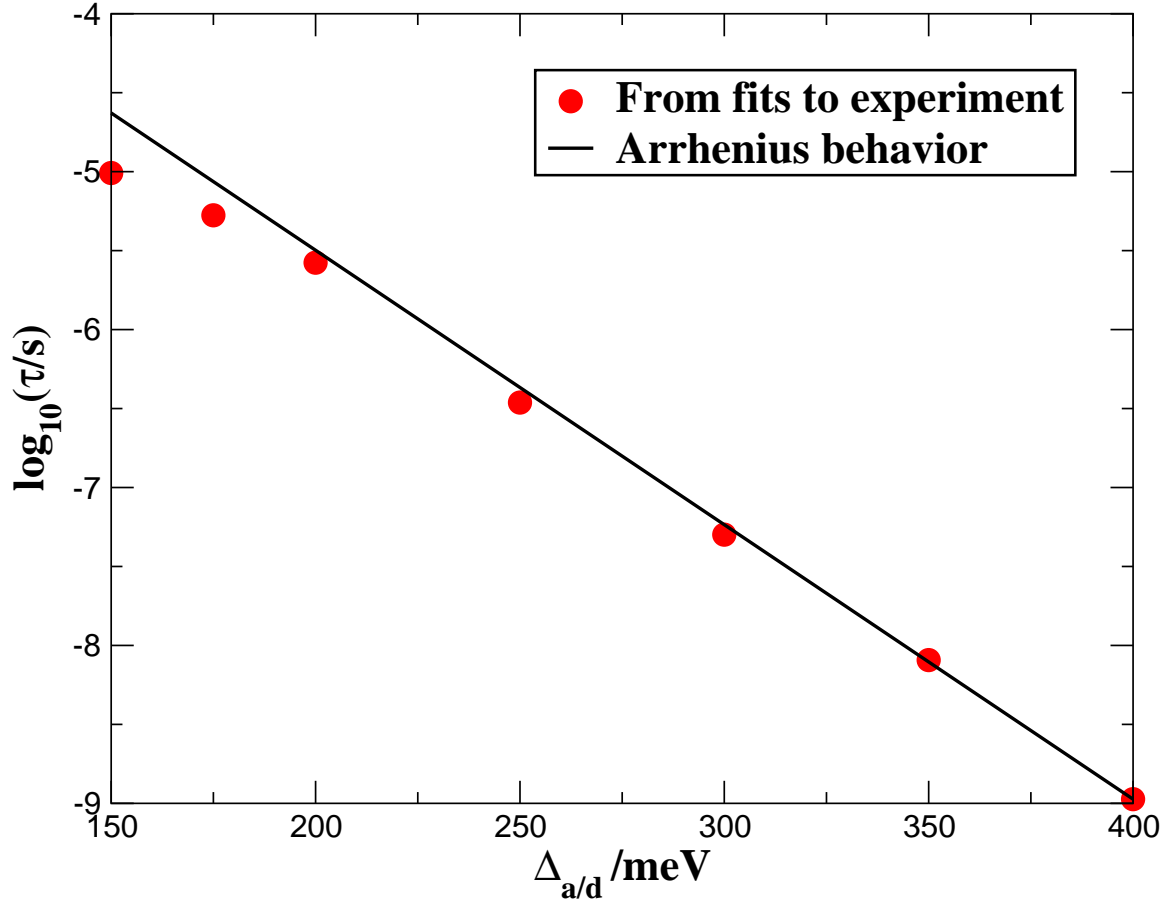


Fig. 4. Arrhenius behavior of $\tau \approx \tau_0 e^{-\beta \Delta_{a/d}}$ as a function of $\Delta_{a/d}$. The slope of the line representing the linear regression of $\log_{10}(\tau/\text{s})$ for $\Delta_{a/d} \geq 200$ meV is $(-0.0388/\ln 10)$ meV $^{-1}$, in very good agreement to what is expected from the Arrhenius equation: $\beta = 0.04$ meV $^{-1}$. As $\Delta_{a/d}$ decreases closer to the values of Δ_{nm} and Δ_{nn} , τ deviates from the Arrhenius behavior.